

Article

Robust Assessment of Macromolecular Fraction (MMF) in Muscle with Differing Fat Fraction Using Ultrashort Echo Time (UTE) Magnetization Transfer Modeling with Measured T1

Saeed Jerban ^{1,2,3,*} , Yajun Ma ^{1,2}, Qingbo Tang ^{1,2}, Eddie Fu ², Nikolaus Szeverenyi ¹, Hyungseok Jang ^{1,2}, Christine B. Chung ^{1,2}, Jiangu Du ^{1,2} and Eric Y. Chang ^{1,2,*} 

¹ Department of Radiology, University of California, La Jolla, San Diego, CA 92093, USA

² Radiology Service, Veterans Affairs San Diego Healthcare System, La Jolla, San Diego, CA 92161, USA

³ Department of Orthopedic Surgery, University of California, La Jolla, San Diego, CA 92093, USA

* Correspondence: sjerban@health.ucsd.edu (S.J.); eric.chang2@va.gov (E.Y.C.); Tel.: +1-858-246-2229 (S.J.); +1-858-642-1221 (E.Y.C.); Fax: +1-888-960-5922 (S.J. & E.Y.C.)

Abstract: Magnetic resonance imaging (MRI) is widely regarded as the most comprehensive imaging modality to assess skeletal muscle quality and quantity. Magnetization transfer (MT) imaging can be used to estimate the fraction of water and macromolecular proton pools, with the latter including the myofibrillar proteins and collagen, which are related to the muscle quality and its ability to generate force. MT modeling combined with ultrashort echo time (UTE-MT modeling) may improve the evaluation of the myotendinous junction and regions with fibrotic tissues in the skeletal muscles, which possess short T2 values and higher bound-water concentration. The fat present in muscle has always been a source of concern in macromolecular fraction (MMF) calculation. This study aimed to investigate the impact of fat fraction (FF) on the estimated MMF in bovine skeletal muscle phantoms embedded in pure fat. MMF was calculated for several regions of interest (ROIs) with differing FFs using UTE-MT modeling with and without T1 measurement and B1 correction. Calculated MMF using measured T1 showed a robust trend, particularly with a negligible error (<3%) for FF < 20%. Around 5% MMF reduction occurred for FF > 30%. However, MMF estimation using a constant T1 was robust only for regions with FF < 10%. The MTR and T1 values were also robust for only FF < 10%. This study highlights the potential of the UTE-MT modeling with accurate T1 measurement for robust muscle assessment while remaining insensitive to fat infiltration up to moderate levels.

Keywords: muscle; MRI; UTE; myotendinous junction; fat infiltration



Citation: Jerban, S.; Ma, Y.; Tang, Q.; Fu, E.; Szeverenyi, N.; Jang, H.; Chung, C.B.; Du, J.; Chang, E.Y. Robust Assessment of Macromolecular Fraction (MMF) in Muscle with Differing Fat Fraction Using Ultrashort Echo Time (UTE) Magnetization Transfer Modeling with Measured T1. *Diagnostics* **2023**, *13*, 876. <https://doi.org/10.3390/diagnostics13050876>

Academic Editor: Anja Müller-Lutz

Received: 12 January 2023

Revised: 17 February 2023

Accepted: 21 February 2023

Published: 24 February 2023



Copyright: © 2023 by the authors. Licensee MDPI, Basel, Switzerland. This article is an open access article distributed under the terms and conditions of the Creative Commons Attribution (CC BY) license (<https://creativecommons.org/licenses/by/4.0/>).

1. Introduction

Magnetic resonance imaging (MRI) is widely regarded as the most comprehensive imaging modality to assess skeletal muscle quality and quantity. Muscle inflammation, fat infiltration, fibrosis, and atrophy are the most common qualitative observations in MR images of muscle injuries and pathologies. Conventional MRI techniques that are routinely performed for qualitative muscle assessments include T1- and T2-weighted [1], short-tau-inversion-recovery [2,3], and diffusion-weighted imaging [4]. However, the standard morphological MRI-based muscle assessments are subjective and may lack reproducibility. Quantitative MRI techniques, including T1 and T2 relaxation times [5–11], magnetization transfer (MT)-related measures [10–18], and diffusion tensor (DT) indices [4,19–21], as well as fat and water separation [22–30], may provide more sensitive, objective, and reproducible measures of the muscle microstructure and composition.

Among the above-mentioned quantitative MRI techniques, MT can provide information on proton pools, such as water and macromolecules, using MT ratio or size estimation of the pools (e.g., macromolecular fraction, MMF) [12,13]. In muscle, the dominant macromolecules include the myofibrillar proteins and collagen, and a measurement of this pool

could be potentially sensitive to the muscle quality and its ability to generate force [31,32]. Using MT techniques, a high-power saturation radio frequency (RF) pulse is used with a predefined frequency different from the water protons' resonance frequency to saturate mainly protons in macromolecules in the skeletal muscle fibers. After the saturation pulse application, the saturated magnetization transfers from the macromolecules to the water protons (bound and free water) that can be detected by MRI as a signal reduction. MT imaging combined with ultrashort echo time (UTE) MRI has been recently introduced as a technique to incorporate the saturations experienced by both free and bound water in different biological tissues [33,34]. UTE-MT modeling may particularly improve the evaluation of the myotendinous junction and regions with fibrotic tissues in the skeletal muscles, which possess short T2 values and higher bound-water concentration. Detecting the applied saturation in such regions of muscle is challenging with conventional MRI sequences that utilize echo times (TEs) greater than a few milliseconds [35]. Accurate MT modeling requires B1 correction and T1 compensation [36]. Remarkably, UTE-MT modeling has been shown to be insensitive to tissue orientation and to provide a robust assessment of musculoskeletal (MSK) tissues regardless of their orientation within the MRI scanner [37].

Fat protons, in theory, should not participate in the MT phenomena because the lipid proton spin group is essentially isolated from the water protons and from the protons on large macromolecules [38]. However, the fat present in muscle has always been a source of concern in MMF calculation and a few studies have reported significant underestimation of MMF for muscles with considerable fat infiltration [16]. This could pose a problem for some applications, such as the rotator cuff musculature in which pathologic muscles can contain up to 30% fat [39]. Robust estimation of MMF in muscle regardless of the macroscopic fat infiltration will be a useful tool for muscle assessment decoupled from the fat infiltration.

The purpose of this study was to investigate the impact of fat fraction (FF) on the estimated MMF in bovine skeletal muscle phantoms embedded in pure fat (lard). MMF was calculated for several regions of interest (ROIs) with differing FFs using UTE-MT modeling with and without T1 measurement and B1 correction.

2. Material and Methods

2.1. Phantom Preparation

Fresh cuts of lean bovine chuck muscles and pure pork fat (lard) were purchased from a local grocery store. The muscle cuts were visually examined to select a lean portion, avoiding the inclusion of obvious interfascicular fat in the prepared muscle specimen. Two muscle sections were placed in a cylindrical plastic container (10 cm in diameter and 20 cm length, approximately). Lard was melted at 60 °C and then cooled to near room temperature. Next, melted lard was poured into the container with the two muscle sections at the bottom. Lard and muscle sections filled up to the middle of the container. The muscle-fat phantom was kept at room temperature until the lard reached its stable solid state. The container was topped with tap water to ensure performing MR imaging at the water peak frequency.

2.2. UTE-MRI Imaging

The 3D-UTE-Cones MRI scans were performed on a 3T MRI scanner (MR750, GE Healthcare Technologies, WI, USA) using an eight-channel knee coil (one RF transmission channel and eight signal reception channels). The muscle-fat container was parallel to the B0 direction of the scanner, and all images were acquired in the coronal plane.

To measure T1 as a prerequisite for the two-pool UTE-MT modeling, the actual flip angle imaging-variable flip angle (AFI-VFA) sequence (AFI: TE = 0.032 ms, TRs = 20, 100 ms, FA = 45°; VFA: TE = 0.032 ms, TR = 20 ms, FAs = 5°, 10°, 20°, and 30°) was performed [40]. Notably, the AFI-VFA sequence results in B1 corrected T1 measurement. A 3D-UTE-Cones-MT sequence (Fermi saturation pulse power = 500°, 1000°, and 1500°; frequency offset = 2, 5, 10, 20, and 50 kHz; FA = 7°; 11 spokes per MT preparation) was performed for MT ratio (MTR) measurement and two-pool MT modeling [34,41]. Field of view, in-plane matrix

dimension, slice thickness, and total scan time were 12 cm, 192×192 , 4 mm, and 35 min, respectively.

2.3. MRI Data Analysis

UTE-MRI analyses were performed initially within seven regions of interest (ROIs) covering only muscle to calculate T1, MTR, and MMF (from MT modeling). Each ROI was then gradually expanded by adding only the neighboring pure fat voxels (lard), which meant increasing FF within ROIs, while the originally included muscle voxels were kept intact. Finally, calculated T1, MTR, and MMFs were plotted against FF values to investigate their estimated variation levels when encountering fat infiltration in muscle. A 5% variation threshold from the original MRI measures (FF = 0) was considered as the range of robustness for each one of the MRI measures. Analyses were performed on a single slice in the middle of the phantom-fat phantom.

A single-component exponential model was used for T1 measurement. The acquired UTE-MT data with the three saturation pulse power levels and the five frequency off-sets were used first for MTR calculation and then two-pool MT modeling to calculate MMF [33,34,41]. MMF calculation was repeated using (1) a constant T1 (T1 = 750 ms, i.e., average T1 values measured in pure muscle regions) and no B1 correction (i.e., B1 = 1), (2) a constant T1 and B1 correction (from the AFI sequence), (3) a measured T1 (from the AFI-VFA sequence) and no B1 correction, and (4) a measured T1 and B1 correction. It should be noted that the measured T1 values used as inputs in MT modeling were B1 corrected (from the AFI-VFA sequence). All UTE MRI measurements and models were performed using MATLAB (version 2021, The Mathworks Inc., Natick, MA, USA) codes developed in-house.

3. Results

Figure 1A demonstrates a T1-weighted UTE MRI image of the bovine muscle specimen embedded in lard (i.e., presumably FF = 100%). Figure 1B,C depict the T1 fitting curves (single component exponential model) on a variable FA dataset for a pure muscle and a pure fat ROI, respectively, both adequately far from the fat/muscle border to avoid partial-volume artifacts.

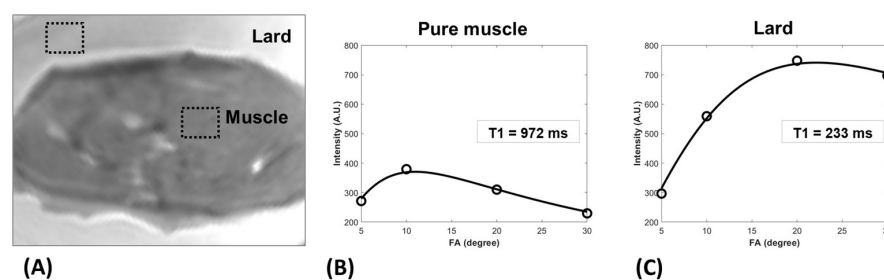


Figure 1. (A) T1-weighted UTE MRI image of a bovine muscle specimen embedded in lard (i.e., FF = 100%). UTE-T1 recovery fitting curves in (B) a pure muscle region of interest (ROI) (T1 = 972 ms) and a (C) pure fat ROI (T1 = 233 ms).

Figure 2A shows an exemplary ROI highlighted in a blue box with an initial FF = 1% that expanded to an ROI with FF = 70% by adding only the neighboring lard voxels (red box) while the muscle compartment of the expanding ROIs was intact. Figure 2B–D depict the UTE-T1 fittings within the three exemplary ROIs shown in Figure 2A (FF = 1, 35 and 70%). T1 values decreased by increasing FF (T1 = 676, 407, and 296 ms for FF = 1, 35 and 70%, respectively).

Figure 3 illustrates the two-pool UTE-MT modeling using a super-Lorentzian function over variable off-resonance frequencies for three different power levels (500° , 1000° , and 1500° power levels are shown in blue, green, and red lines) within four exemplary ROIs with (A1–A4) FF = 0 (pure muscle far from fat border, Figure 1A), (B1–B4) FF = 1% (Figure 2A),

(C1–C4) 35% (Figure 2A), and (D1–D4) FF = 70% (Figure 2A). MT modeling was repeated four times using (1) a constant T1 ($T_1 = 750$ ms) and no B1 correction, (2) a constant T1 and B1 correction, (3) a measured T1 and no B1 correction, and (4) a measured T1 and B1 correction. The actual signal changes within all investigated ROIs were fitted reasonably well using all the calculation methods.

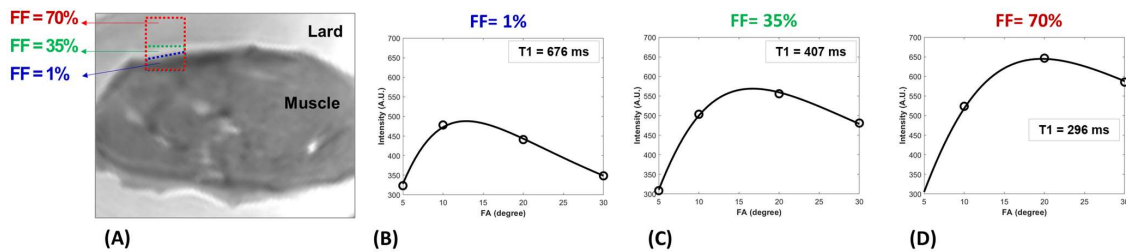


Figure 2. (A) T1-weighted UTE MRI image of the bovine muscle specimen embedded in lard. The blue box (dotted line) indicates an exemplary ROI with $FF \approx 1\%$ that expanded by only adding the neighboring lard voxels up to $FF = 35\%$ (green box, dotted line) and then $FF = 70\%$ (red box, dotted line). UTE-T1 recovery fitting curves for the ROI with (B) $FF = 1\%$ ($T_1 = 676$ ms), (C) $FF = 35\%$ ($T_1 = 407$ ms), and (D) $FF = 70\%$ ($T_1 = 296$ ms).

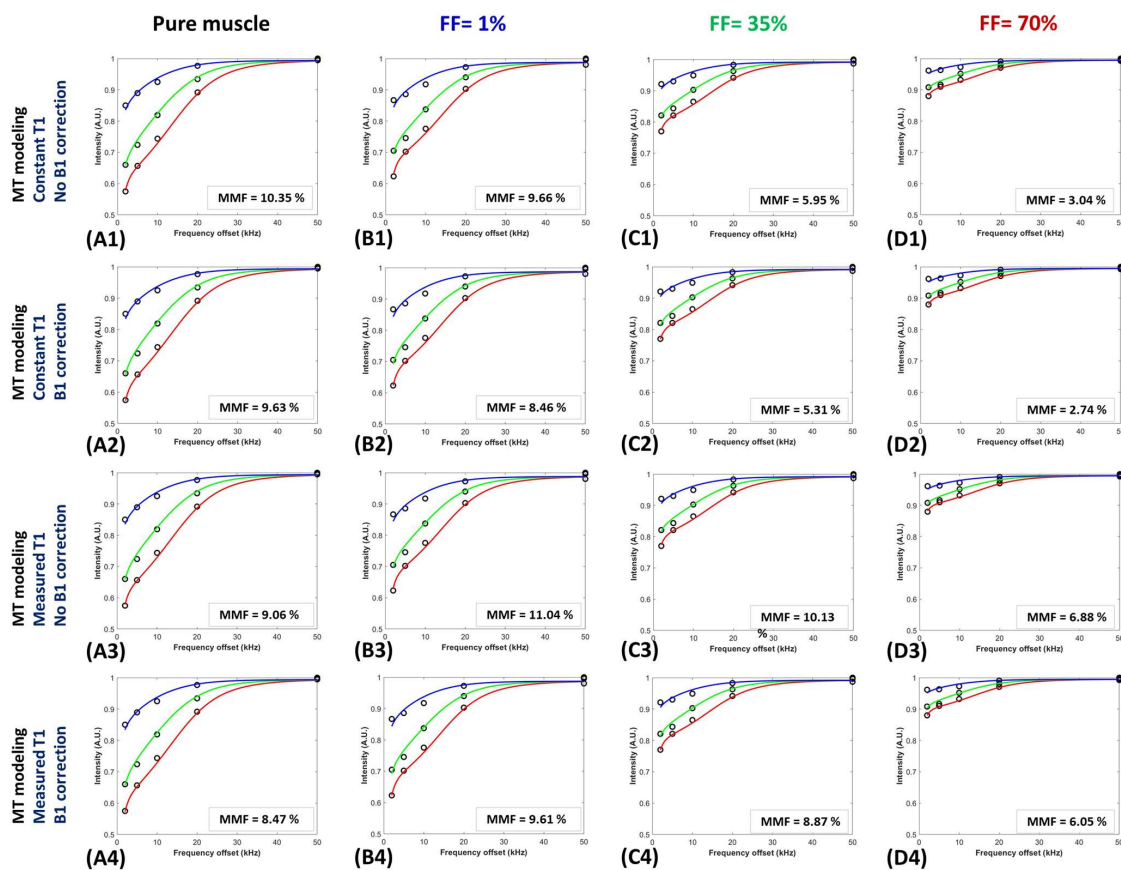


Figure 3. Two-pool UTE-MT modeling using a super-Lorentzian function over variable off-resonance frequencies for three different power levels (500° , 1000° , and 1500° power levels are shown in blue, green, and red lines) within four exemplary ROIs with (A1–A4) $FF = 0$ (pure muscle far from fat border, Figure 1A), (B1–B4) $FF = 1\%$ (Figure 2A), (C1–C4) 35% (Figure 2A), and (D1–D4) $FF = 70\%$ (Figure 2A). MT modeling was repeated using (1) a constant T1 ($T_1 = 750$ ms, i.e., average T1 values measured in pure muscle regions) and no B1 correction (i.e., $B_1 = 1$), (2) a constant T1 and B1 correction (from the AFI sequence), (3) a measured T1 (from the AFI-VFA sequence) and no B1 correction, and (4) a measured T1 and B1 correction.

Figure 4 depicts T1 and MTR as well as their normalized values versus FF within the seven series of ROIs initiated with pure muscle ROIs with FF = 0% and expanded to ROIs up to FF = 70% by adding only neighboring pure lard voxels. T1 and MTR decreased by more than 5% for FF values above 10%. For ROIs with 50% fat content, T1 and MTR decreased to around 40% to 60% of their original values.

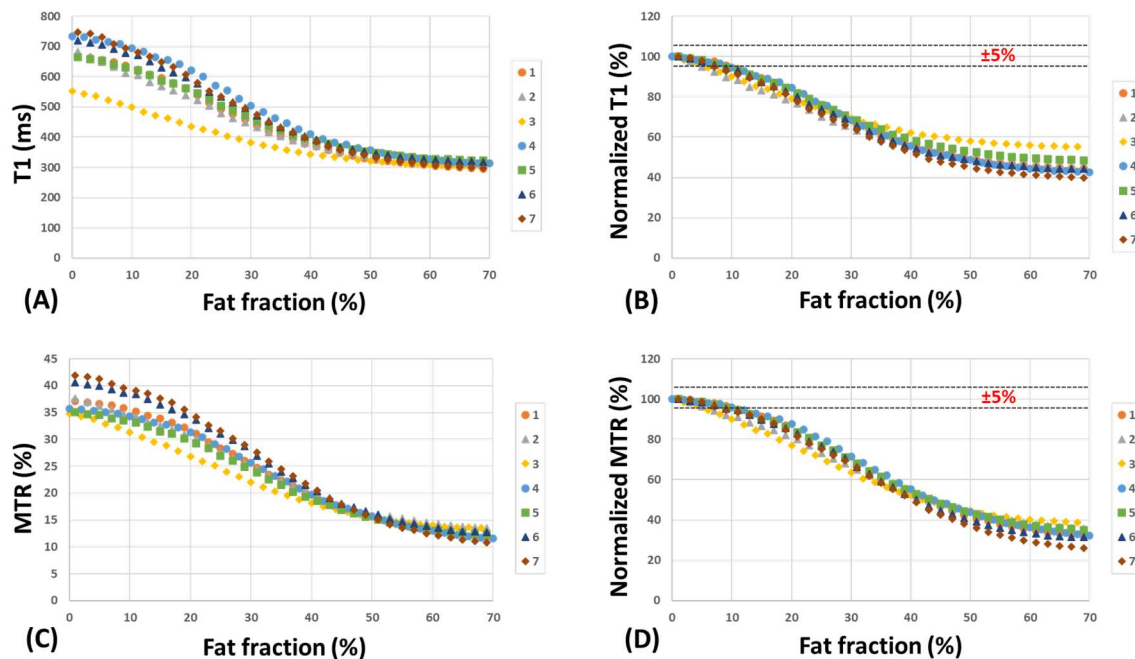


Figure 4. (A) T1 (ms) and (B) normalized T1 (%) versus FF within seven series of ROIs initiated with pure muscle ROIs (FF \approx 0%) on the fat border and expanded by adding only neighboring pure lard voxels (FF up to 70%). (C) MTR (%) and (D) normalized MTR (%) versus FF within the same ROIs. T1 and MTR decreased by more than 5% for FF above 10%.

Figure 5 shows MMF and normalized MMF values versus FF within the seven expanding ROIs (FF = 0 to 70%) using the four calculation methods used in Figure 3. MMF decreased by more than 5% for FF above 10% when constant T1 (T1 = 750 ms) was used (Figure 5A–D). However, when the measured T1 was used (E–H), the 5% MMF reduction occurred for FF > 30%. MMF calculated with the measured T1 showed a much more robust trend, particularly with a less than 3% error for FF < 20%. For ROIs with 50% fat content, the MMF error stayed below 30% when the accurately measured T1 was used in the calculation.

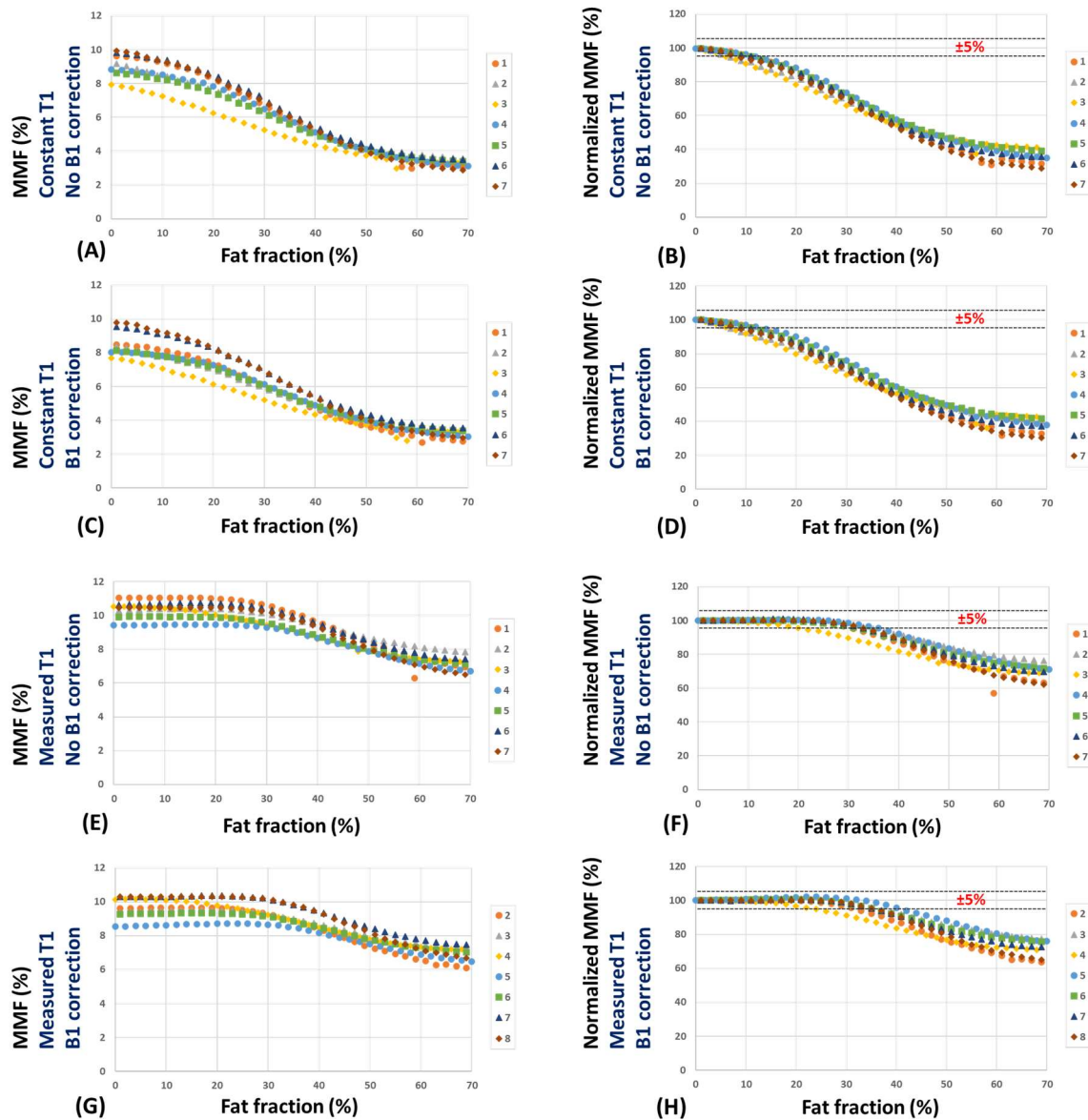


Figure 5. MMF and normalized MMF values versus FF within the seven expanding ROIs (FF = 0 to 70%) using (A,B) a constant T1 (T1 = 750 ms) and no B1 correction, (C,D) a constant T1 and B1 correction, (E,F) a measured T1 (from the AFI-VFA sequence) and no B1 correction, and (G,H) a measured T1 and B1 correction. MMF decreased by more than 5% for FF above 10% when constant T1 (T1 = 750 ms) was used (A–D). However, when an accurately measured T1 was used (E–H), the 5% MMF reduction occurred for FF > 30%. The calculated MMF using a measured T1 showed a less than 3% error for FF < 20%.

4. Discussion

The impact of fat content on the MMF estimations from UTE-MT modeling was investigated using a muscle/lard phantom. The estimated MMF from UTE-MT modeling using the accurately measured T1 demonstrated a robust trend and showed under 5% changes for muscle/fat ROIs with FF up to 30%. The MMF underestimation was less than 3% for regions with FF < 20%.

This study highlighted the potential of the two-pool UTE-MT modeling with the T1 compensation method for robust protein content estimation as a measure of muscle quality while remaining insensitive to fat infiltration up to moderate levels. This could be a particularly useful technique for some applications, such as analyzing rotator cuff

musculature where pathologic muscles can contain up to 30% fat [39]. Notably, MMF estimation using constant T1 was robust only for regions with FF < 10%. The MTR and T1 values were also robust only for FF < 10%.

The presence of fat in muscle results in an apparent decrease in measured MT effect, which is demonstrated as decreases in MTR (Figure 4C,D) and MMF using constant T1 (Figure 5A,B). On the other hand, as shown in Supplementary Figure S1, for a pure muscle ROI, decreasing the T1 value results in an overestimation of the MMF of muscle (increasing from around 9% to 24% by T1 decrease from 1000 ms to 300 ms). Such an overestimation in MMF was likely compensating for the apparent MT effect reductions caused by fat infiltration in our phantom study, which, in turn, led to the robust MMF values for a large range of FF (up to 30%) when the measured net T1 (including muscle and fat) was used in the models.

Robust estimation of MMF in muscle regardless of the macroscopic fat infiltration can decouple the muscle assessment from the fat infiltration, which may impair the muscle performance independently in the case of injuries and pathologies. Remarkably, UTE-MT modeling has been shown previously to be insensitive to tissue orientation and to provide a robust assessment of MSK tissues regardless of their orientation within the MRI scanner [37]. Being less sensitive to the tissue orientation and the macroscopic fat-infiltration makes the UTE-MT technique a useful tool for muscle assessment, particularly in the myotendinous junction and regions with fibrotic tissues. It should be noted that UTE-MT modeling has been previously used mainly to assess MSK tissues with significant fractions of short T2 components, such as cartilage [42,43], meniscus [42], ligament [44], tendon [45–47], and bone [48–52].

MMF in muscle is potentially sensitive to the muscle quality and its ability to generate force. The fat present in muscle has always been a source of concern in MMF calculation. Li et al. have demonstrated significant underestimation in MMF values by increasing FF through a set of numerical simulations of MT pulses [16]. Therefore, using MT sequences combined with fat saturation methods has been suggested in previous studies to avoid MMF underestimations [11,15,16]. However, fat saturation preparation can create challenges. For instance, the fat saturation pulse may attenuate signals from tissues with short T2 relaxation times because of their broad frequency spectrum that may overlap with the main fat signal peak [53]. In addition, the pulse may generate magnetization transfer effects [54], which can result in increases in MMF measurement [11].

Several other quantitative MRI techniques have been reported in the literature for muscle assessments. T1 and T2 measurements have been used for muscle injury and pathology assessment and aging-related differences in several investigations [5–8,10]. Briefly, T1 values were found to be higher in muscle inflammation regions while they are lower in fat-infiltrated regions [5]. T2 values, however, were found to be higher in both muscle inflammation and fat-infiltrated regions [9]. DT imaging in MR has been widely used to evaluate the diffusion preference directions by the water molecules in tissues with well-organized long fibers, such as muscles, tendons, and ligaments. DT indices can provide information about the tissue microstructure and fibers' orientation at a microscopic level. The diffusion properties of muscle, especially the third eigenvalue of the diffusion tensor and degree of diffusion anisotropy, reflect muscle damage due to injury [19,20] and disease [4,21]. Moreover, since macroscopic fat infiltration is a widespread observation in muscle pathologies and injuries, several studies have been devoted to performing an accurate estimation of the fat content in tissues, with most employing the different frequencies of fat and water protons [22–30].

The limitations of this study can be summarized in three aspects. First, the number of samples was small as is the nature of pilot studies. Second, bovine rather than human muscle tissue was used because bovine muscle could be readily obtained in a fresh and non-diseased state. Third, since the original muscle cuts were not performed by the authors, identifying the exact muscles of the bovine chuck (with more than 20 muscles) was not possible in this study. Considerable differences in fat and collagen composition among

the muscles [55] and within each specific muscle [56] may affect the estimated MMF values. Although biochemical or microstructural analyses were not performed to confirm a minimum fat content in the muscle cuts, the selected ROIs were in regions that appeared devoid of macroscopic fat. Fourth, this study was performed ex vivo on a uniform muscle/fat phantom. The presence of nonuniform fat with irregular shapes and other soft and hard tissues, lower spatial resolution, a higher body temperature [57], and subject motion may all contribute to the reduced performance of all UTE-MRI-based imaging techniques in vivo compared with ex vivo studies. Fifth, this study was focused on macroscopic fat infiltration in muscle as limited by the current phantom study design. Future investigations should be performed to investigate the potential impacts of microscopic fat infiltration in muscle, which might require accurate and well-developed fat saturation or water excitation techniques [58].

5. Conclusions

Robust estimation of MMF in muscle regardless of the macroscopic fat infiltration can decouple the muscle assessment from the fat infiltration. The estimated MMF from UTE-MT modeling using the accurately measured T1 demonstrated a robust trend and showed under 5% changes for muscle/fat ROIs with FF up to 30%. MMF using a constant T1 value, similar to MTR showed robust values only for ROIs with FF < 10%. This study highlighted the potential of the UTE-MT modeling with the T1 compensation method for robust skeletal muscle assessment.

Supplementary Materials: The following supporting information can be downloaded at: <https://www.mdpi.com/article/10.3390/diagnostics13050876/s1>, Figure S1: The relation between MMF in muscle and the input T1 value.

Author Contributions: Conceptualization, E.Y.C. and S.J.; methodology, S.J., Y.M., Q.T, E.F., N.S., H.J., J.D. and E.Y.C.; software, S.J. and Y.M.; formal analysis, S.J.; investigation, S.J., Y.M., N.S., H.J., J.D., C.B.C. and E.Y.C.; resources, J.D., C.B.C. and E.Y.C.; data curation, S.J., Q.T. and E.F.; writing—original draft preparation, S.J., Y.M. and E.Y.C.; writing—review and editing, S.J., Y.M., Q.T, E.F., N.S., H.J., C.B.C., J.D. and E.Y.C.; visualization, S.J.; supervision, E.Y.C. All authors have read and agreed to the published version of the manuscript.

Funding: The authors acknowledge grant support from the Veterans Affairs Clinical Science and Biomedical R&D (I01CX001388, I01BX005952, and I01CX000625), National Institutes of Health (K01AR080257, R01AR068987, R01AR062581, R01AR075825, R01AR079484, and 5P30AR073761), and GE Healthcare.

Institutional Review Board Statement: Not applicable.

Informed Consent Statement: Not applicable.

Data Availability Statement: Data supporting the reported results can be provided by the corresponding authors upon courtesy request.

Conflicts of Interest: The authors have no conflict of interest to declare.

References

1. Kaufman, L.D.; Gruber, B.L.; Gerstman, D.P.; Kaell, A.T. Preliminary Observations on the Role of Magnetic Resonance Imaging for Polymyositis and Dermatomyositis. *Ann. Rheum. Dis.* **1987**, *46*, 569–572. [[CrossRef](#)] [[PubMed](#)]
2. Curiel, R.V.; Jones, R.; Brindle, K. Magnetic Resonance Imaging of the Idiopathic Inflammatory Myopathies: Structural and Clinical Aspects. *Ann. N. Y. Acad. Sci.* **2009**, *1154*, 101–114. [[CrossRef](#)]
3. Kimball, A.B.; Summers, R.M.; Turner, M.; Dugan, E.M.; Hicks, J.; Miller, F.W.; Rider, L.G. Magnetic Resonance Imaging Detection of Occult Skin and Subcutaneous Abnormalities in Juvenile Dermatomyositis: Implications for Diagnosis and Therapy. *Arthritis Rheum.* **2000**, *43*, 1866–1873. [[CrossRef](#)] [[PubMed](#)]
4. Qi, J.; Olsen, N.J.; Price, R.R.; Winston, J.A.; Park, J.H. Diffusion-Weighted Imaging of Inflammatory Myopathies: Polymyositis and Dermatomyositis. *J. Magn. Reson. Imaging* **2008**, *27*, 212–217. [[CrossRef](#)]

5. Park, J.H.; Olsen, N.J.; King, L.K., Jr.; Vital, T.; Buse, R.; Kari, S.; Schulman, M.H.; Price, R.R. Use of Magnetic Resonance Imaging and P-31 Magnetic Resonance Spectroscopy to Detect and Quantify Muscle Dysfunction in the Amyopathic and Myopathic Variants of Dermatomyositis. *Arthritis Rheum.* **1995**, *38*, 68–77. [[CrossRef](#)] [[PubMed](#)]
6. Huang, Y.; Majumdar, S.; Genant, H.K.; Chan, W.P.; Sharma, K.R.; Yu, P.; Mynhier, M.; Miller, R.G. Quantitative MR Relaxometry Study of Muscle Composition and Function in Duchenne Muscular Dystrophy. *J. Magn. Reson. Imaging* **1994**, *4*, 59–64. [[CrossRef](#)]
7. Kim, H.K.; Laor, T.; Horn, P.S.; Racadio, J.M.; Wong, B.; Dardzinski, B.J. T2 Mapping in Duchenne Muscular Dystrophy: Distribution of Disease Activity and Correlation with Clinical Assessments. *Radiology* **2010**, *255*, 899–908. [[CrossRef](#)]
8. Arpan, I.; Forbes, S.C.; Lott, D.J.; Senesac, C.R.; Daniels, M.J.; Triplett, W.T.; Deol, J.K.; Sweeney, H.L.; Walter, G.A.; Vandendorpe, K. T2 Mapping Provides Multiple Approaches for the Characterization of Muscle Involvement in Neuromuscular Diseases: A Cross-Sectional Study of Lower Leg Muscles in 5-15-Year-Old Boys with Duchenne Muscular Dystrophy. *NMR Biomed.* **2013**, *26*, 320–328. [[CrossRef](#)]
9. Fan, R.H.; Does, M.D. Compartmental Relaxation and Diffusion Tensor Imaging Measurements in Vivo in λ -Carrageenan-Induced Edema in Rat Skeletal Muscle. *NMR Biomed.* **2008**, *21*, 566–573. [[CrossRef](#)]
10. White, J.C.; Sinha, S.; Sinha, U. Spin Lattice (T1) and Magnetization Transfer Saturation (MTsat) Imaging to Monitor Age-Related Differences in Skeletal Muscle Tissue. *Diagnostics* **2022**, *12*, 584. [[CrossRef](#)]
11. Chen, Y.; Li, L.; Le, N.; Chang, E.Y.; Huang, W.; Ma, Y.J. On the Fat Saturation Effect in Quantitative Ultrashort TE MR Imaging. *Magn. Reson. Med.* **2022**, *87*, 2388–2397. [[CrossRef](#)] [[PubMed](#)]
12. Sinclair, C.D.J.; Samson, R.S.; Thomas, D.L.; Weiskopf, N.; Lutti, A.; Thornton, J.S.; Golay, X. Quantitative Magnetization Transfer in in Vivo Healthy Human Skeletal Muscle at 3 T. *Magn. Reson. Med.* **2010**, *64*, 1739–1748. [[CrossRef](#)] [[PubMed](#)]
13. McDaniel, J.D.; Ulmer, J.L.; Prost, R.W.; Franczak, M.B.; Jaradeh, S.; Hamilton, C.A.; Mark, L.P. Magnetization Transfer Imaging of Skeletal Muscle in Autosomal Recessive Limb Girdle Muscular Dystrophy. *J. Comput. Assist. Tomogr.* **1999**, *23*, 609–614. [[CrossRef](#)]
14. Bajd, F.; Škrlep, M.; Čandek-Potokar, M.; Vidmar, J.; Serša, I. Application of Quantitative Magnetization Transfer Magnetic Resonance Imaging for Characterization of Dry-Cured Hams. *Meat Sci.* **2016**, *122*, 109–118. [[CrossRef](#)] [[PubMed](#)]
15. Romero, I.O.; Sinha, U. Magnetization Transfer Saturation Imaging of Human Calf Muscle: Reproducibility and Sensitivity to Regional and Sex Differences. *J. Magn. Reson. Imaging* **2019**, *50*, 1227–1237. [[CrossRef](#)] [[PubMed](#)]
16. Li, K.; Dortch, R.D.; Kroop, S.F.; Huston, J.W.; Gochberg, D.F.; Park, J.H.; Damon, B.M. A Rapid Approach for Quantitative Magnetization Transfer Imaging in Thigh Muscles Using the Pulsed Saturation Method. *Magn. Reson. Imaging* **2015**, *33*, 709–717. [[CrossRef](#)] [[PubMed](#)]
17. Li, K.; Dortch, R.D.; Welch, E.B.; Bryant, N.D.; Buck, A.K.W.; Park, J.H. Multi-parametric MRI Characterization of Healthy Human Thigh Muscles at 3.0 T—Relaxation, Magnetization Transfer, Fat/Water, and Diffusion Tensor Imaging. *NMR Biomed.* **2014**, *27*, 1070–1084. [[CrossRef](#)] [[PubMed](#)]
18. Nuñez-Peralta, C.; Montesinos, P.; Alonso-Jiménez, A.; Alonso-Pérez, J.; Reyes-Leiva, D.; Sánchez-González, J.; Llauger-Roselló, J.; Segovia, S.; Belmonte, I.; Pedrosa, I.; et al. Magnetization Transfer Ratio in Lower Limbs of Late Onset Pompe Patients Correlates with Intramuscular Fat Fraction and Muscle Function Tests. *Front. Neurol.* **2021**, *12*, 634766. [[CrossRef](#)]
19. McMillan, A.B.; Shi, D.; Pratt, S.J.P.; Lovering, R.M. Diffusion Tensor MRI to Assess Damage in Healthy and Dystrophic Skeletal Muscle after Lengthening Contractions. *J. Biomed. Biotechnol.* **2011**, *2011*, 970726. [[CrossRef](#)] [[PubMed](#)]
20. Zaraiskaya, T.; Kumbhare, D.; Noseworthy, M.D. Diffusion Tensor Imaging in Evaluation of Human Skeletal Muscle Injury. *J. Magn. Reson. Imaging* **2006**, *24*, 402–408. [[CrossRef](#)]
21. Heemskerk, A.M.; Strijkers, G.J.; Drost, M.R.; van Bochove, G.S.; Nicolay, K. Skeletal Muscle Degeneration and Regeneration after Femoral Artery Ligation in Mice: Monitoring with Diffusion MR Imaging. *Radiology* **2007**, *243*, 413–421. [[CrossRef](#)] [[PubMed](#)]
22. Glover, G.H. Multipoint Dixon Technique for Water and Fat Proton and Susceptibility Imaging. *J. Magn. Reson. Imaging* **1991**, *1*, 521–530. [[CrossRef](#)] [[PubMed](#)]
23. Yu, H.; McKenzie, C.A.; Shimakawa, A.; Vu, A.T.; Brau, A.C.S.; Pineda, A.R.; Beatty, P.J.; Brittain, J.H.; Reeder, S.B. Multiecho Reconstruction for Simultaneous Water-Fat Decomposition and T2* Estimation. *J. Magn. Reson. Imaging* **2007**, *26*, 1153–1161. [[CrossRef](#)]
24. Reeder, S.B.; Wen, Z.; Yu, H.; Pineda, A.R.; Gold, G.E.; Markl, M.; Pelc, N.J. Multicoil Dixon Chemical Species Separation with an Iterative Least-Squares Estimation Method. *Magn. Reson. Med.* **2004**, *51*, 35–45. [[CrossRef](#)] [[PubMed](#)]
25. Yu, H.; Shimakawa, A.; McKenzie, C.A.; Brodsky, E.; Brittain, J.H.; Reeder, S.B. Multiecho Water-Fat Separation and Simultaneous R² Estimation with Multifrequency Fat Spectrum Modeling. *Magn. Reson. Med.* **2008**, *60*, 1122–1134. [[CrossRef](#)] [[PubMed](#)]
26. Schlaeger, S.; Sollmann, N.; Zoffl, A.; Becherucci, E.A.; Weidlich, D.; Kottmaier, E.; Riederer, I.; Greve, T.; Montagnese, F.; Deschauer, M.; et al. Quantitative Muscle MRI in Patients with Neuromuscular Diseases—Association of Muscle Proton Density Fat Fraction with Semi-Quantitative Grading of Fatty Infiltration and Muscle Strength at the Thigh Region. *Diagnostics* **2021**, *11*, 1056. [[CrossRef](#)]
27. Grimm, A.; Meyer, H.; Nickel, M.D.; Nittka, M.; Raithel, E.; Chaudry, O.; Friedberger, A.; Uder, M.; Kemmler, W.; Engelke, K.; et al. A Comparison between 6-Point Dixon MRI and MR Spectroscopy to Quantify Muscle Fat in the Thigh of Subjects with Sarcopenia. *J. Frailty Aging* **2019**, *8*, 21–26. [[CrossRef](#)]
28. Ma, J. A Single-Point Dixon Technique for Fat-Suppressed Fast 3D Gradient-Echo Imaging with a Flexible Echo Time. *J. Magn. Reson. Imaging* **2008**, *27*, 881–890. [[CrossRef](#)]

29. Jang, H.; Carl, M.; Ma, Y.; Jerban, S.; Guo, T.; Zhao, W.; Chang, E.Y.; Du, J. Fat Suppression for Ultrashort Echo Time Imaging Using a Single-Point Dixon Method. *NMR Biomed.* **2019**, *32*, e4069. [[CrossRef](#)]
30. Berglund, J.; Johansson, L.; Ahlström, H.; Kullberg, J. Three-Point Dixon Method Enables Whole-Body Water and Fat Imaging of Obese Subjects. *Magn. Reson. Med.* **2010**, *63*, 1659–1668. [[CrossRef](#)]
31. Willingham, T.B.; Kim, Y.; Lindberg, E.; Bleck, C.K.E.; Glancy, B. The Unified Myofibrillar Matrix for Force Generation in Muscle. *Nat. Commun.* **2020**, *11*, 3722. [[CrossRef](#)] [[PubMed](#)]
32. Haus, J.M.; Carrithers, J.A.; Carroll, C.C.; Tesch, P.A.; Trappe, T.A. Contractile and Connective Tissue Protein Content of Human Skeletal Muscle: Effects of 35 and 90 Days of Simulated Microgravity and Exercise Countermeasures. *Am. J. Physiol.* **2007**, *293*, R1722–R1727. [[CrossRef](#)] [[PubMed](#)]
33. Ma, Y.; Shao, H.; Du, J.; Chang, E.Y. Ultrashort Echo Time Magnetization Transfer (UTE-MT) Imaging and Modeling: Magic Angle Independent Biomarkers of Tissue Properties. *NMR Biomed.* **2016**, *29*, 1546–1552. [[CrossRef](#)] [[PubMed](#)]
34. Ma, Y.; Chang, E.Y.; Carl, M.; Du, J. Quantitative Magnetization Transfer Ultrashort Echo Time Imaging Using a Time-Efficient 3D Multispike Cones Sequence. *Magn. Reson. Med.* **2017**, *79*, 692–700. [[CrossRef](#)]
35. Chang, E.Y.; Du, J.; Chung, C.B. UTE Imaging in the Musculoskeletal System. *J. Magn. Reson. Imaging* **2015**, *41*, 870–883. [[CrossRef](#)]
36. Ma, Y.; Lu, X.; Carl, M.; Zhu, Y.; Szeverenyi, N.M.; Bydder, G.M.; Chang, E.Y.; Du, J. Accurate T 1 Mapping of Short T 2 Tissues Using a Three-Dimensional Ultrashort Echo Time Cones Actual Flip Angle Imaging-Variable Repetition Time (3D UTE-Cones AFI-VTR) Method. *Magn. Reson. Med.* **2018**, *80*, 598–608. [[CrossRef](#)] [[PubMed](#)]
37. Zhu, Y.; Cheng, X.; Ma, Y.; Wong, J.H.; Xie, Y.; Du, J.; Chang, E.Y. Rotator Cuff Tendon Assessment Using Magic-Angle Insensitive 3D Ultrashort Echo Time Cones Magnetization Transfer (UTE-Cones-MT) Imaging and Modeling with Histological Correlation. *J. Magn. Reson. Imaging* **2018**, *48*, 160–168. [[CrossRef](#)] [[PubMed](#)]
38. Sobol, W.T.; Cameron, I.G.; Inch, W.R.; Pintar, M.M. Modeling of Proton Spin Relaxation in Muscle Tissue Using Nuclear Magnetic Resonance Spin Grouping and Exchange Analysis. *Biophys. J.* **1986**, *50*, 181–191. [[CrossRef](#)]
39. Nardo, L.; Karampinos, D.C.; Lansdown, D.A.; Carballido-Gamio, J.; Lee, S.; Maroldi, R.; Ma, C.B.; Link, T.M.; Krug, R. Quantitative Assessment of Fat Infiltration in the Rotator Cuff Muscles Using Water-Fat MRI. *J. Magn. Reson. Imaging* **2014**, *39*, 1178–1185. [[CrossRef](#)] [[PubMed](#)]
40. Ma, Y.J.; Zhao, W.; Wan, L.; Guo, T.; Searleman, A.; Jang, H.; Chang, E.Y.; Du, J. Whole Knee Joint T1 Values Measured in Vivo at 3T by Combined 3D Ultrashort Echo Time Cones Actual Flip Angle and Variable Flip Angle Methods. *Magn. Reson. Med.* **2019**, *81*, 1634–1644. [[CrossRef](#)] [[PubMed](#)]
41. Ma, Y.; Tadros, A.; Du, J.; Chang, E.Y. Quantitative Two-Dimensional Ultrashort Echo Time Magnetization Transfer (2D UTE-MT) Imaging of Cortical Bone. *Magn. Reson. Med.* **2018**, *79*, 1941–1949. [[CrossRef](#)]
42. Jerban, S.; Kasibhatla, A.; Ma, Y.; Wu, M.; Chen, Y.; Guo, T.; Wan, L.; Szeverenyi, N.; Chang, E.Y.; Du, J. Detecting Articular Cartilage and Meniscus Deformation Effects Using Magnetization Transfer Ultrashort Echo Time (MT-UTE) Modeling during Mechanical Load Application: Ex Vivo Feasibility Study. *Cartilage* **2020**, *8*, 665S–673S. [[CrossRef](#)]
43. Namiranian, B.; Jerban, S.; Ma, Y.; Dorthe, E.W.; Masoud-Afsahi, A.; Wong, J.H.; Zhao, W.; Wei, Z.; Chen, Y.; D’Lima, D.; et al. Assessment of Mechanical Properties of Articular Cartilage with Quantitative Three-Dimensional Ultrashort Echo Time (UTE) Cones Magnetic Resonance Imaging. *J. Biomech.* **2020**, in press. [[CrossRef](#)] [[PubMed](#)]
44. Jerban, S.; Hananouchi, T.; Ma, Y.; Namiranian, B.; Dorthe, E.W.; Wong, J.H.; Shojaeiadib, N.; Wu, M.; Du, J.; D’Lima, D.; et al. Correlation between the Elastic Modulus of Anterior Cruciate Ligament (ACL) and Quantitative Ultrashort Echo Time (UTE) Magnetic Resonance Imaging. *J. Orthop. Res.* **2022**, *40*, 2330–2339. [[CrossRef](#)] [[PubMed](#)]
45. Aria Ashir, B.S.; Ma, Y.; Jerban, S.; Jang, H.; Wei, Z.; Nicole Le, B.A.; Du, J.; Chang, E.Y. Rotator Cuff Tendon Assessment in Symptomatic and Control Groups Using Quantitative MRI. *J. Magn. Reson. Imaging* **2020**, *52*, 864–872. [[CrossRef](#)] [[PubMed](#)]
46. Jerban, S.; Ma, Y.; Afsahi, A.M.; Lombardi, A.; Wei, Z.; Shen, M.; Wu, M.; Le, N.; Chang, D.G.; Chung, C.B.; et al. Lower Macromolecular Content in Tendons of Female Patients with Osteoporosis versus Patients with Osteopenia Detected by Ultrashort Echo Time (UTE) MRI. *Diagnostics* **2022**, *12*, 1061. [[CrossRef](#)]
47. Jerban, S.; Ma, Y.; Namiranian, B.; Ashir, A.; Shirazian, H.; Zhao, W.; Wu, M.; Cai, Z.; Le, N.; Du, J.; et al. Age-Related Decrease in Collagen Proton Fraction in Tibial Tendons Estimated by Magnetization Transfer Modeling of Ultrashort Echo Time Magnetic Resonance Imaging (UTE-MRI). *Sci. Rep.* **2019**, *9*, 17974. [[CrossRef](#)]
48. Jerban, S.; Ma, Y.; Wong, J.H.; Nazaran, A.; Searleman, A.; Wan, L.; Williams, J.; Du, J.; Chang, E.Y. Ultrashort Echo Time Magnetic Resonance Imaging (UTE-MRI) of Cortical Bone Correlates Well with Histomorphometric Assessment of Bone Microstructure. *Bone* **2019**, *123*, 8–17. [[CrossRef](#)] [[PubMed](#)]
49. Jerban, S.; Ma, Y.; Dorthe, E.W.; Kakos, L.; Le, N.; Alenezi, S.; Sah, R.L.; Chang, E.Y.; D’Lima, D.; Du, J. Assessing Cortical Bone Mechanical Properties Using Collagen Proton Fraction from Ultrashort Echo Time Magnetization Transfer (UTE-MT) MRI Modeling. *Bone Rep.* **2019**, *8*, 100220. [[CrossRef](#)] [[PubMed](#)]
50. Jerban, S.; Ma, Y.; Wan, L.; Searleman, A.C.; Jang, H.; Sah, R.L.; Chang, E.Y.; Du, J. Collagen Proton Fraction from Ultrashort Echo Time Magnetization Transfer (UTE-MT) MRI Modelling Correlates Significantly with Cortical Bone Porosity Measured with Micro-computed Tomography (MCT). *NMR Biomed.* **2019**, *32*, e4045. [[CrossRef](#)] [[PubMed](#)]
51. Jerban, S.; Ma, Y.; Li, L.; Jang, H.; Wan, L.; Guo, T.; Searleman, A.; Chang, E.Y.; Du, J. Volumetric Mapping of Bound and Pore Water as Well as Collagen Protons in Cortical Bone Using 3D Ultrashort Echo Time Cones MR Imaging Techniques. *Bone* **2019**, *127*, 120–128. [[CrossRef](#)] [[PubMed](#)]

52. Jerban, S.; Ma, Y.; Nazaran, A.; Dorthe, E.W.; Cory, E.; Carl, M.; D’Lima, D.; Sah, R.L.; Chang, E.Y.; Du, J.; et al. Detecting Stress Injury (Fatigue Fracture) in Fibular Cortical Bone Using Quantitative Ultrashort Echo Time-Magnetization Transfer (UTE-MT): An Ex Vivo Study. *NMR Biomed.* **2018**, *31*, e3994. [[CrossRef](#)] [[PubMed](#)]
53. Carl, M.; Nazaran, A.; Bydder, G.M.; Du, J. Effects of Fat Saturation on Short T2 Quantification. *Magn. Reson. Imaging* **2017**, *43*, 6–9. [[CrossRef](#)] [[PubMed](#)]
54. Henkelman, R.M.; Stanisz, G.J.; Graham, S.J. Magnetization Transfer in MRI: A Review. *NMR Biomed.* **2001**, *14*, 57–64. [[CrossRef](#)]
55. Seggern, D.D.V.; Calkins, C.R.; Johnson, D.D.; Brickler, J.E.; Gwartney, B.L. Muscle Profiling: Characterizing the Muscles of the Beef Chuck and Round. *Meat Sci.* **2005**, *71*, 39–51. [[CrossRef](#)]
56. Picard, B.; Gagaoua, M.; Gagaoua, M. Muscle Fiber Properties in Cattle and Their Relationships with Meat Qualities: An Overview. *J. Agric. Food Chem.* **2020**, *68*, 6021–6039. [[CrossRef](#)]
57. Jerban, S.; Szeverenyi, N.; Ma, Y.; Guo, T.; Namiranian, B.; To, S.; Jang, H.; Chang, E.Y.; Du, J. Ultrashort Echo Time MRI (UTE-MRI) Quantifications of Cortical Bone Varied Significantly at Body Temperature Compared with Room Temperature. *Investig. Magn. Reson. Imaging* **2019**, *23*, 202–209. [[CrossRef](#)]
58. Ma, Y.; Jerban, S.; Jang, H.; Chang, E.Y.; Du, J. Fat Suppression for Ultrashort Echo Time Imaging Using a Novel Soft-hard Composite Radiofrequency Pulse. *Magn. Reson. Med.* **2019**, *82*, 2178–2187. [[CrossRef](#)]

Disclaimer/Publisher’s Note: The statements, opinions and data contained in all publications are solely those of the individual author(s) and contributor(s) and not of MDPI and/or the editor(s). MDPI and/or the editor(s) disclaim responsibility for any injury to people or property resulting from any ideas, methods, instructions or products referred to in the content.